Understanding XANES spectra of two-temperature warm dense copper using *ab initio* simulation.

N. Jourdain,[1,2] V. Recoules,[1] L. Lecherbourg,[1,3] P. Renaudin,[1] and F. Dorchies[2]

[1] *CEA-DAM-DIF, F-91297 Arpajon, France*
[2] *Univ. Bordeaux, CNRS, CEA, CELIA, UMR 5107, F-33400 Talence, France*
[3] *LOA, ENSTA ParisTech, CNRS, EcolePolytechnique, Université Paris-Saclay, 91120 Palaiseau, France*

(Dated: February 1, 2022)

Using *ab initio* molecular–dynamics simulations combined with linear–response theory, we studied the x–ray absorption near–edge spectra (XANES) of a two-temperature dense copper plasma. As the temperature increases, XANES spectra exhibit a pre–edge structure balanced by a reduction of the absorption just behind the edge. By performing systematic simulations for various thermodynamic conditions, we establish a formulation to deduce the electronic temperature T_e directly from the spectral integral of the pre–edge that can be used for various thermodynamic conditions encountered in a femtosecond heating experiment where thermal non–equilibrium and expanded states have to be considered.

arXiv:2002.05561v1 [cond-mat.mtrl-sci] 13 Feb 2020

Time resolved X-ray absorption near-edge spectroscopy (TR-XANES) was recently extended to the Warm Dense Matter (WDM) regime [1]. This highly transient physics has required specific development to get an appropriate time-resolution (picosecond or less) on XANES measurements. TR-XANES gives a complete picture by probing simultaneously the valence electrons and the atomic local arrangement modifications in WDM situations well beyond the melting. However, the physical interpretation of XANES spectra is not straightforward and a strong connection between theory and experiment is needed to extract information. This issue has been addressed using *ab initio* molecular dynamics (AIMD) simulations, providing a consistent description of both the electronic and ionic structures, together with X-ray absorption spectra calculation [2, 3].

In the past decade, both theoretical and experimental XANES spectroscopy was used to get a deep understanding of the electronic structure modification of metals in the WDM. On aluminum, XANES modification during the solid–liquid–vapor phase transition was observed with picosecond time-resolution [7]. With the support of AIMD simulations, this has shown the connection between electronic and ionic modifications. Comparison between measurements and calculations for molybdenum have demonstrated that XANES spectra can be simply interpreted in terms of electron DOS modification when solid molybdenum turns to WDM [5]. Besides the understanding of the phenomena involved, it is possible to have access to the timescales of phase transitions [4, 6, 7]. XANES spectra were also used to shed light on the DOS modification induced by laser shock compression in metals such as aluminum [8, 9] and iron [10, 11].

When WDM is transiently produced by femtosecond laser heating, matter faces non equilibrium situations. It is a great scientific challenge to independently resolve the electron and ion dynamics. In principle, TR–XANES can address this physics, but it is necessary to disentangle the corresponding features in XANES spectra, which depend on the considered element. In some light metals such as Be [14] and Al [15], the electronic temperature can be retrieved directly from the slope of the absorption K edge. In most metals with a localized d band, the situation is more complex and this methodology cannot be applied. Recent experiments have been dedicated to femtosecond laser heated warm dense copper on a synchrotron beamline [3, 12]. Using 2 ps time resolved X-ray spectroscopy, Cho et al investigated the modification of XANES spectra near $L_{2,3}$ edge. By direct comparison between measured spectra and spectra computed using AIMD, they retrieved the time evolution of the electron temperature and compare it to the behaviour obtained using a two-temperature models.

The purpose of the present paper is to go further in the calculations and analysis of warm dense copper using AIMD simulations. The interpretation of XANES spectra especially for transition metal is non trivial and require a careful analysis. The relation between the electronic temperature T_e and pre–edge peak is reproduced. A quasi linear function is extracted to deduce absolute values of T_e (up to 3 eV) from the spectral integration of the pre–edge. The impacts of ion temperature T_i and density are carefully and independently studied. This shows the validity of this function in the various thermodynamic conditions encountered in a femtosecond heating experiment, including strong thermal non equilibrium. This provides a practical T_e diagnostic to analyze any XANES experiment without the need of additional AIMD calculations. It has been used in a recently published paper that revisits the electron–ion thermal equilibration dynamics on a table–top set up, emphasizing the critical role of target expansion [13]. Other features are identified above L-edge, in close relation with the crystalline structure.

I. XANES SPECTRUM AT AMBIENT CONDITION

Before analyzing the modification of XANES spectra induced by electron temperature (T_e), ion temperature (T_i), and density $_rho$, we first need a clear understand-

ing of the connection between XANES spectra and the electronic structure of copper at ambient condition. This is also a way to check the validity and the precision of the method we use.

A. Computational method

To obtain X-ray absorption spectra of warm dense copper, we first need to generate a set of atomic configurations for a given (ρ,T_i,T_e) condition. AIMD simulations are performed using the *ab initio* plane wave Density Functional Theory (DFT) code ABINIT [16–18]. DFT is applied together with Local Density Approximation [19]. For non-equilibrium AIMD simulations the ion and electron temperatures are controlled independently. While the electron temperature is fixed for every time step in the simulation, the ion temperature is controlled in the iso-kinetics ensemble where the velocity is rescaled at every time step to maintain the desired temperature.

We start the simulations with 108 atoms initially arranged in a perfect fcc lattice. The equilibration for a given temperature is then monitored by looking at the pressure. Before reaching a stable ionic structure, the system relaxes for a few hundreds of time steps during which the pressure increases. After equilibration, it fluctuates around a well–defined value. At the end, the initial configuration is propagated up to 2 ps using time steps of 2 fs for the low temperature and 0.5 fs for temperatures above 1 eV. We consider electronic states occupied down to 10^{-6} electrons per states which means around 1 600 bands are explicitly computed for the highest temperature considered here. All molecular dynamics calculations were performed at the Γ point to represent the Brillouin zone. The Γ point sampling is expected to be a good approximation for the calculation of the structure and dynamics of copper. We use for this element a PAW data set generated using 11 outer electrons ($3d^{10}4s^1$) and a cut–off radius of 2 bohr that has been benchmarked against physical properties obtained from experiments [20]. The plane wave cut–off is 15 Ha.

We then select equally spaced ionic configurations along the equilibrated part of the trajectory and compute for each of them the corresponding electronic structure with a DFT calculation. These *ab initio* electronic structure calculations are performed on a $3\times3\times3$ Monkhorst-Pack **k**–point grid and with 2 500 electronic bands in order to obtain eigenstates converged up to 50 eV above the chemical potential. For this part, the PAW data set includes semi–core states with 19 outer electrons ($3s^2 3p^6 3d^{10} 4s^1$) and a cut–off radius of 2 bohr [20]. Two projectors are used for s and p channels, and three projectors for the d channel. The plane wave cut–off is 25 Ha. These electronic structure calculations provide all the required outputs to compute the absorption cross section.

The absorption cross section is calculated in a single electron picture: an electron make the transition from a core orbital ϕ_{core} to an excited state $\psi_{n,\mathbf{k}}$. The transition energy corresponds to the energy difference between these orbitals. Then, for a given $\boldsymbol{k}$-point, the absorption cross section is expressed as [21]:

$$\sigma_{\mathbf{k}}(\omega) = 4\pi^2\omega \sum_n [1 - f(\epsilon_{n,\mathbf{k}})] \times |\langle\psi_{n,\mathbf{k}}|\vec{\nabla}|\phi_{core}\rangle|^2 \delta(\epsilon_{core} - \epsilon_n - \hbar\omega) \quad (1)$$

We employ atomic units, with the electron charge e, Planck's constant $\hbar$, the electron mass m_e, and the fine structure constant α all set to unity. The n summation ranges over the discrete bands (orbitals). $f(\epsilon_{n,\mathbf{k}})$ is the Fermi-Dirac occupation factor corresponding to the energy $\epsilon_{n,\mathbf{k}}$ of the nth band and for the **k**–point **k**. The total cross section is obtained by direct summation over all necessary **k**–points.

To take into account the natural linewidth of the levels involved in the transition and the resulting spectral broadening of the absorption edges, we use a Lorentzian function to model the delta function of equation 1:

$$\delta(\epsilon_{core} - \epsilon_n - \hbar\omega) = \frac{1}{\pi} \frac{\Gamma_f(\omega)}{\Gamma_f(\omega)^2 + (\epsilon_{core} - \epsilon_n - \hbar\omega)^2} \quad (2)$$

This Lorentzian function has an energy-dependent width Γ_f according to the reference [22] which reads :

$$\Gamma_f(\omega) = \begin{cases} 0, & \hbar\omega < E_F \\ \Gamma_{\boldsymbol{hole}} + \gamma(\omega), & \hbar\omega > E_F \end{cases} \quad (3)$$

This reproduces structures at the L_2 edge broader than the ones at the L_3 edge.

In equation 3, $\Gamma_{\boldsymbol{hole}}$ is the core level spectral width. The γ function is an arctangent like function that gives a smooth broadening from $\Gamma_{\boldsymbol{hole}}$ to a chosen $\Gamma_{\boldsymbol{max}}$ value, and is expressed as:

$$\gamma(\omega) = \Gamma_{\boldsymbol{max}} \left[\frac{1}{2} + \frac{1}{\pi}\arctan\left(e - \frac{1}{e^2}\right)\right] \quad (4)$$

where $e = (\omega - E_F)/(E_{ctr} - E_F)$ and E_{ctr} is the inflection point of the arctangent function.

The core states $|\phi_{core}\rangle$ are obtained from an all-electron atomic calculation performed during the generation of our PAW data set using Atompaw code [23]. For the $L_{2,3}$ absorption edge which we consider here, we need the ϕ_{2p} orbitals. The radial part of $2p_{1/2}$ and $2p_{3/2}$ core wave function are taken identical. The spin-orbit splitting of the $2p$ states is introduced by shifting the calculated absorption spectrum by the value of the energy separation between the L_3 and the L_2 edges. It can be obtained from a DFT relativistic all–electron calculation and is equal to 20 eV. The two edges have similar structures, but their intensities are related by a factor of 2 (the statistical branching ratio). Left panel of figure 1 shows how the L_2 edge is constructed from the L_3 edge for the XANES spectrum at ambient conditions.

During the experimental measurements of the XANES spectra, the system is modified by the probe itself as an

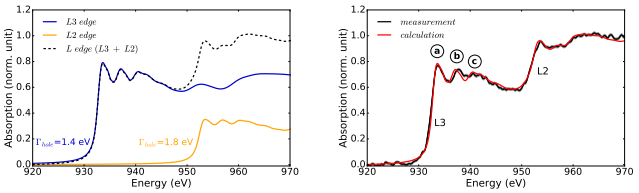


FIG. 1. (color online). *Left panel* : Construction of the total XANES spectrum at $L_{2,3}$ absorption edges from the spectrum calculated at L_3 edge for the case in ambient conditions (ρ_0, $T_e = T_i = 300$ K). *Right panel* : Calculation (red curve) of the XANES spectrum at $L_{2,3}$ absorption edges of copper at normal solid density $\rho_0 = 8.9$ g/cm^3 and at $T_e = T_i = 300$ K compared to experiment in the same conditions (black curve).

inner–shell electron is removed. In many cases [24], it is necessary to include in the simulation cell one atom described by a PAW data set including a hole in the core shell. This is a way to model the electron–hole interaction but it neglects many body interactions and dynamic core-hole interaction. In the case of copper, the agreement with the experimental spectrum is better without the consideration of the core hole. This was already observed in ref [22]. Quoting Mauchamp *et al.* [24], a core-hole effect is always present in any core-level spectroscopy experiment but its effect is not always evidenced and nothing can be said a priori concerning the agreement or not with the experiment. When building PAW dataset with a hole in the core, there is no mean to test those PAW datasets. The only way is to compare directly the XANES spectra with experiment. This was also the choice in ref [3, 12].

At the end, we compute absorption cross section for each atom in the simulation box for each snapshot and then do an average on the resulting spectra.

B. Comparison with experiment

The right panel of figure 1 shows the comparison between the theoretical and the experimental [13] XANES spectra in ambient conditions. The absolute position of the edge can not be formally obtained with the present model. To be compared with the experiment, the theoretical spectrum for the cold case is shifted to match the experimental energy position of the edge. The same rigid shift will then be applied to all computed absorption spectra.

The best agreement with the experimental cold spectrum is obtained using $\Gamma_{\boldsymbol{hole}} = 1.4$ eV and $\Gamma_{\boldsymbol{max}} = 5.1$ eV for the L_3 edge. For the L_2 edge, we use a fixed value of 1.8 eV. These values of Γ_{hole} are close to the one found in the reference [25] taken into account the spectral resolution of the experimental spectrum. These values are used for all computed spectra and can be seen in Figure 1 for both L_3 and L_2 edges.

The agreement between experimental and theoretical spectra is excellent. The first three peaks above the L_3 edge (labeled (a), (b) and (c)) and the minimum around 950 eV are well reproduced. The spectral shape and amplitude of the L_2 edge are also well described by the theoretical spectrum.

$L_{2,3}$ edges probe the unoccupied s and d states. This is illustrated in the Figure 2 showing the density of states projected on s and d channels together with the corresponding XANES spectrum at the L_3 edge. p states are not shown here as they do not contribute to the absorption cross section because of the selection rule $\Delta l = \pm 1$. For copper at ambient conditions, the $3d$ states are entirely occupied and the XANES spectrum reflects the s and d type orbitals above the chemical potential $\mu(T_e)$. The colored areas in Figure 2 refer to the unoccupied DOS which is representative of the possible final states of the photoelectron transition. On this shaded part, we recognize the features in the electron DOS that are responsible for the three peaks (a), (b) and (c) localized between 930 eV and 940 eV in the XANES spectrum, as well as the minimum amplitude at $\sim$ 20 eV above $\mu(T_e = 300$ K).

II. SHAPE MODIFICATIONS INDUCED BY TEMPERATURE.

To identify the shape modifications induced by the rise of the temperature, we carry out calculations of the x-ray absorption spectrum for several electronic and ionic temperatures at solid density. However, hydrodynamic expansion of thin targets can become significant after only few picoseconds in ultrafast pump-probe experiments. To take this into account, we carry out simulations for density below the solid density to see if this density change has some influence on the modification induced by temperature.

A. Temperature dependence: at thermal equilibrium $T_e = T_i$

We start by simulations at thermal equilibrium where $T_e = T_i$ at solid density $\rho_0 = 8.9$ g/cm^3. Computed XANES spectra for temperatures up to 2 eV are reported on the upper panel of Figure 3. For the temperature of 0.25 eV, the copper is melted (the melting being expected at 0.117 eV = 1358 K at ambient pressure).

As the temperature increases, a pre–edge peak appears and is partially balanced by a reduction of the absorption just behind the edge. This behavior was also observed in ref [12] for temperature up to 2 eV. The intensity of this pre–edge structure is connected to the value of the electrons temperature T_e. When increasing T_e, some electrons from the $3d$-band, fully occupied in ambient conditions, are promoted towards higher energy states and above $\mu(T_e)$. Thus, the vacant states created below $\mu(T_e)$

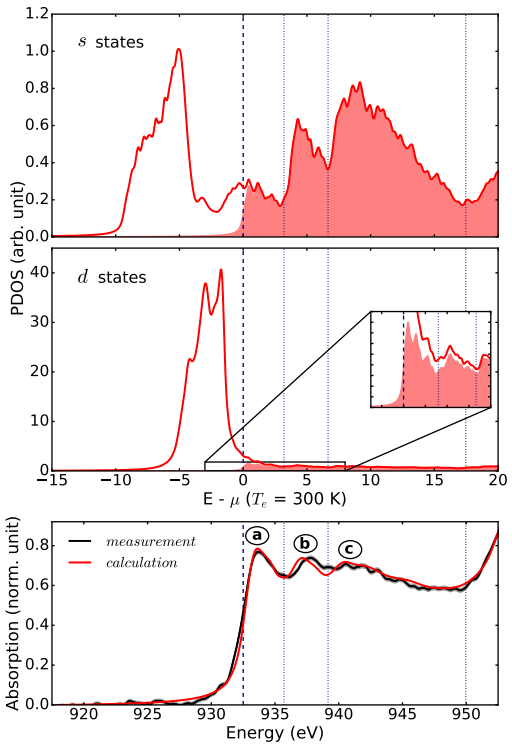


FIG. 2. (color online). *Upper panel:* Projected density of states (PDOS) for copper at normal solid density ρ_0 and at $T_e = T_i = 300$ K for s and d channels. The colored areas correspond to the vacant electronic states. The d channel is zoomed because of the high amplitude of the $3d$-band localized ~ 1.5 eV below $\mu(T_e = 300\text{ K})$. *Lower panel:* Calculation of the XANES spectrum at L_3 absorption edges of copper (red curve) compared to experiment in the same conditions (black curve).

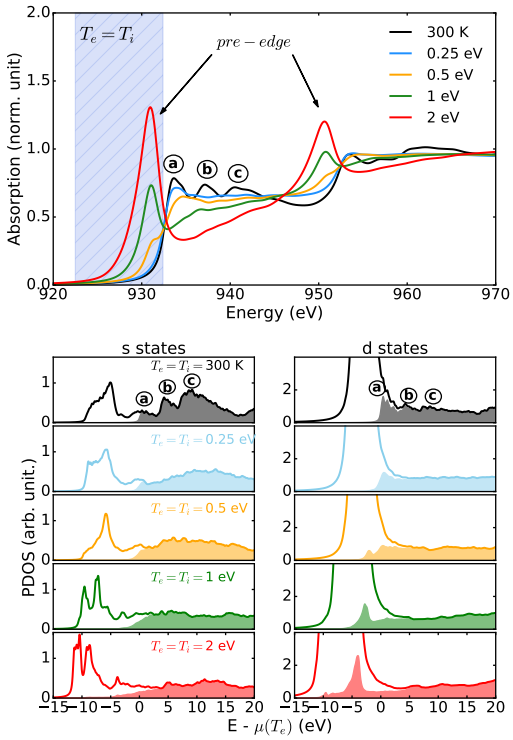


FIG. 3. (color online). *Upper panel:* *ab initio* XANES spectra at $L_{2,3}$ absorption edges of copper at normal solid density $\rho_0 = 8.9$ g/cm^3 and at thermal equilibrium $T_e = T_i$ up to $T_e = 2$ eV. *Lower panel:* Corresponding projected density of states (PDOS) on s and d channels. The colored areas correspond to the vacant electronic states.

become available for photoionization. $2p \rightarrow 3d$ transitions are then possible, and this induces the formation of a pre–edge structure in the XANES spectrum. This was observed that for transition metals, the $L_{2,3}$ white line intensity can be explained on the basis of d vacancies [26]. This is also true for copper. The size of the pre–edge is connected to the shape of the electronic occupation, governed by Fermi-Dirac distribution $f(\epsilon, \mu(T_e), T_e)$ defined as:

$$f(\epsilon, \mu(T_e), T_e) = \frac{1}{1 + \exp\left(\dfrac{\epsilon - \mu(T_e)}{k_b T_e}\right)} \qquad (5)$$

It depends on both the energy ϵ, the chemical potential $\mu(T_e)$ and the temperature T_e. The $3d$-band is highly localized at ambient condition and keeps this property even at high temperatures as can be seen in the lower panel of Figure 3. Copper has an fcc crystalline structure at normal conditions, and the local environment does not change strongly upon melting. The empty part of the $3d$-band consequently appears as a thin peak also beyond melting temperature.

The absorption spectrum becomes however different above the edge. A loss of spectral structures in this region is clearly observed in the Figure 3 for $T_e = T_i \geq 0.25$ eV, in close correlation with the loss of DOS structures above $\mu(T_e)$ in the liquid state. As soon as the system turns to liquid, the structures labeled (b) and (c) on the XANES spectra and the PDOS vanish. The first peak (a) stays visible up to 0.5 eV and then disappears as the absorption is reduced in this region. The structures (b) and (c) might then be used to detect the loss of crystalline structure in copper but this would require further analysis to consolidate this observation. Note that these (b) and (c) structures are not comparable to EXAFS oscillation observable around 30eV above the edge which are connected to diffusion of photo–electrons on the neighbour atoms.

B. Electronic temperature dependence at $T_e \neq T_i = 300K$

To enhance the effect of T_e on the spectra without any influence from the atomic structure, we now focus on

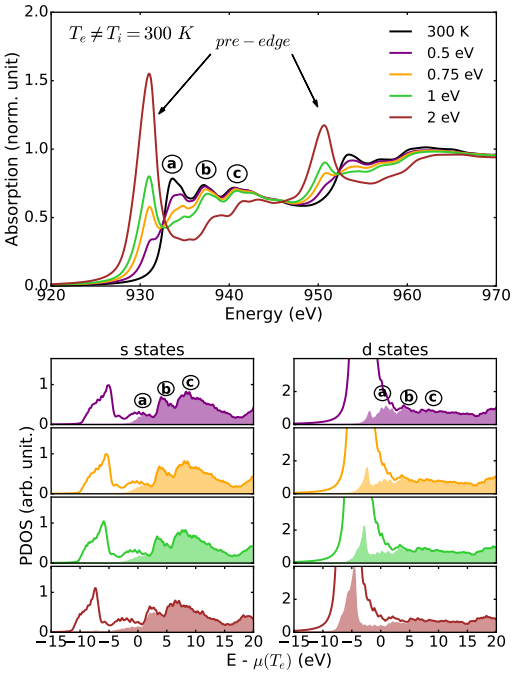


FIG. 4. (color online). *Upper panel:* *ab initio* XANES spectra at $L_{2,3}$ absorption edges of copper at solid density ρ_0 = 8.9 g/cm^3 for strong out-of-equilibrium conditions $T_e \gg T_i$ = 300 K up to T_e = 2 eV. *Lower panel:* Corresponding projected density of states (PDOS) on s and d channels. The colored areas correspond to the vacant electronic states.

the electronic temperature dependence of the XANES spectra by performing simulations at different T_e up to 2 eV while keeping T_i at 300 K at the solid density ρ_0. The ionic structure is the fcc one obtained for the ions at 300 K. The computed spectra are presented on the upper panel of Figure 4. As for the case $T_e = T_i$, the broadening of Fermi-Dirac distribution with T_e always leads to the depopulation of electronic states at the top of the 3d–band.

The structure referred as (a) on these absorption spectra is strongly reduced as the electronic temperature T_e increases. The structures labeled (b) and (c) stay clearly visible up to the highest temperature simulated here.

The lower panel of Figure 4 shows the corresponding s and d components of the PDOS. When increasing the electronic temperature T_e while keeping the same crystalline atomic structure, the general shape of the 3d-band is nearly unchanged. This is also true for the s component. The structures in the projected DOS connected to the peaks (b) and (c) of the XANES spectra are visible for all temperatures T_e. This confirms that the (b) and (c) structures are directly linked to the ionic structure, and that the pre–edge and structure (a) are representative of the electronic temperature T_e.

The DOS shape is different between thermally equilibrated and strong out-of-equilibrium cases (presented latter in the Fig. 7). When copper turns from out-of-equilibrium fcc (ions at 300 K) to liquid at thermal equilibrium ($T_e = T_i$), the 3d-band stays localized but its shape is modified. That leads to slightly higher amplitude and thinner pre–edge structures for a given T_e when T_i = 300 K. This can be seen by comparing the corresponding XANES spectra shown in Figures 3 and 4. In all cases, areas stay comparable.

C. Temperature dependence for expanded cases $\rho < \rho_0$

The question is now to evaluate the effect of the density on the signature of temperature in XANES spectra. Simulations for three different density values were therefore performed: at solid density ρ_0 = 8.9 g/cm^3, liquid density ρ_{liquid} = 8 g/cm^3 and at an expanded density of 6 g/cm^3.

Figure 5 shows the computed XANES spectra for the expanded case at ρ = 6 g/cm^3 and for equilibrated temperatures $T_e = T_i$ up to 2 eV. We also observe the rise of the pre–edge structure with the electronic temperature T_e. Its amplitude value for a given temperature is slightly higher compared to XANES calculations at the solid density ρ_0 reported in Figures 3 and 4. The pre–edge is also thiner and the absorption level is lower above the absorption edge.

To interpret these observations, one can refer to the Figure 6 showing the DOS for several densities as a function of $\epsilon - \mu(T_e)$. It appears that the 3d-band is not strongly modified, with both temperature and density. Therefore, the Fermi-Dirac distribution has similar impact on the 3d-band occupation. This is clearly visible in the shaded areas showing the unoccupied DOS. The pre–edge structure keeps a similar shape in the absorption spectra at these lower densities (*e.g.* at ρ = 6 g/cm^3 in Figure 5).

Looking more closely at Figure 6, the 3d-band gets thinner at lower density and leads to a higher amplitude of the right side of this electronic band. Consequently, for a given temperature, the pre–edge amplitude becomes higher when the density decreases.

III. XANES SPECTRA SHIFTS

The positions of the pre–edge and other peaks above the edge in the absorption spectrum are connected to the energy difference between the DOS and the 2p orbital. Both undergo variations with temperature and density that we have to take into account to describe a possible energy shift of the absorption features when modifying the thermodynamical conditions. This is mandatory to be able to compare theoretical and experimental spectra.

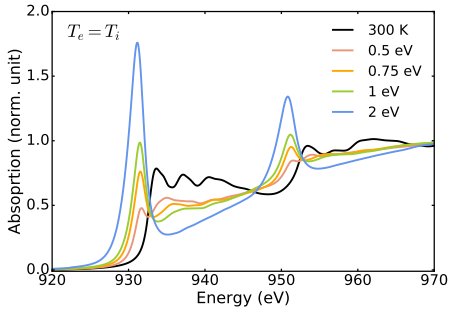


FIG. 5. (color online). XANES spectra at ambient conditions and for different temperatures in equilibrated situations ($T_e = T_i$) for the expanded density $\rho = 6$ g/cm^3.

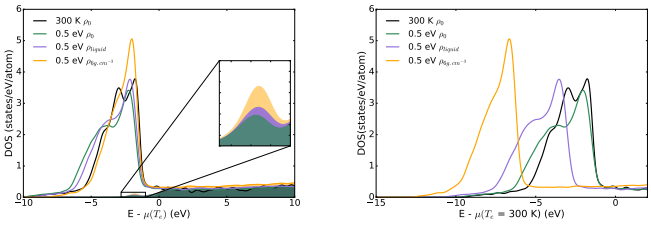


FIG. 6. (color online). left panel: Density of States (DOS) of copper at different densities for $T_e = T_i = 0.5$ eV and compared to the one at ambient conditions. They are represented as a function of $\epsilon - \mu(T_e)$. The colored areas correspond to the vacant electronic states. The inset shows a zoom of the region inside the square around -2.5 eV. Right panel : same DOS represent as a function of constant $\epsilon - \mu(T_e = 300K)$

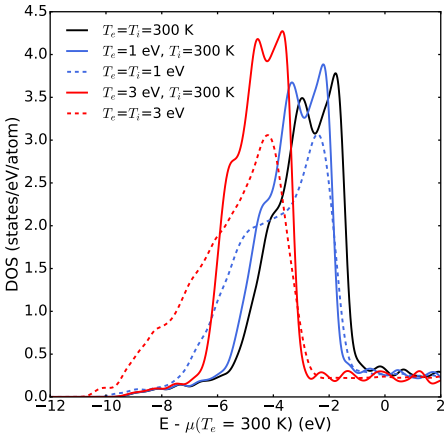


FIG. 7. (color online). Density of States (DOS) of copper at solid density ρ_0 for both thermally equilibrated ($T_e = T_i$) and strong out-of-equilibrium ($T_e \gg T_i = 300$ K) conditions up to 3 eV.

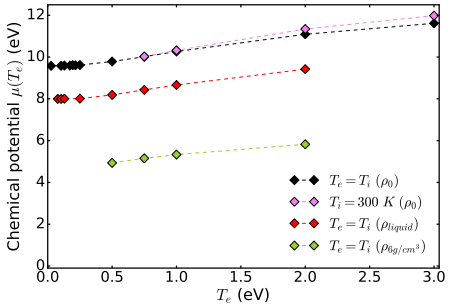


FIG. 8. (color online). Evolution of the chemical potential $\mu(T_e)$ with the temperature of the electrons T_e for three densities of copper $\rho = \rho_0, \rho = \rho_{liquid} = 8$ g/cm^3 and $\rho = 6$ g/cm^3.

A. DOS and chemical potential shifts with temperature and density

A negative shift of the DOS is observed when the density is fixed and the temperature is increased. This effect is shown in the Figure 7 for the solid density ρ_0 and different temperatures, in both thermally equilibrated ($T_e = T_i$) and strong out-of-equilibrium ($T_e \gg T_i = 300$ K) situations. For a given electronic temperature, the energy shift is identical for these two situations.

The energy shift of the chemical potential $\mu(T_e)$ is directly correlated to the DOS one, since $\mu(T_e)$ is obtained by the conservation of the total number of electrons $N_e = \int g(\varepsilon, T) f(\varepsilon, \mu(T_e), T) d\varepsilon$ with $g(\varepsilon, T)$ the electronic DOS and $f(\varepsilon, \mu(T_e), T)$ the Fermi-Dirac distribution. As can be observed on figure 8, the chemical potential increases with temperature and exceeds from around 2 eV its ambient value at $T_e = 3$ eV and this is true for both cases $T_e = T_i$ and $T_e \gg T_i = 300$ K. Given the similar motions between these two cases, we might reasonably assume that the number of electrons in these localized $3d$ bands is not different for a given temperature. The broadening of the Fermi-Dirac distribution and the negative DOS shift lead to an increase of the chemical potential. This was observed for transition metals with localized d states [27, 28]. This is the opposite of the motion of the chemical potential computed for aluminum and this could be traced back to the free-electrons like behaviour of aluminum [2].

When the density is lowered, the density of states is also shifted towards lower energies for a given temperature as can be seen in the right panel of figure 6.

In parallel, the chemical potential drops due to the conservation of the total number of electrons N_e (see Figure 8). In the expanded case, the $3d$ states are even more localized than for the case at normal density. This was already observed for aluminum, where delocalized states becomes more atomic like when density decreases. As a consequence, the chemical potential has to decrease to recover the right number of electrons for a given temper-

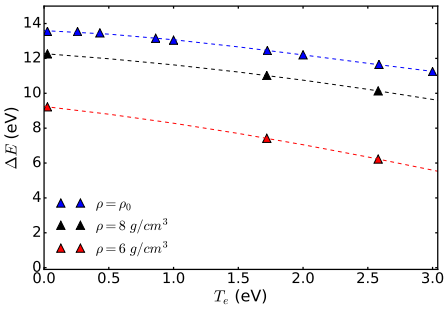


FIG. 9. (color online). Evolution of the energy difference ΔE between $2p$ orbital energies when considered in the frozen core or not. ΔE is defined as $E(2p_{relaxed}) - E(2p_{atomic})$ where $E(2p_{atomic})$ corresponds to the value when the $2p$ orbital is frozen.

ature [9]. This is a density effect. For a given density, even for the lowest density explored here, the chemical potential still increases with temperature.

B. *2p* orbital relaxation

When changes in temperature and/or density occur, the $2p$ orbitals relax to different energies. This can result in possible XANES spectra shifts if the probed valence electronic states do not shift accordingly. This was observed for expanded aluminum and molybdenum [5, 9].

We recall that all XANES calculations involve the frozen core approximation. The generation of the PAW dataset using Atompaw and the energy value of the core orbitals result from an atomic calculation. To take into account the relaxation we generate a different PAW data set where only $1s$ states are frozen. Relative variations ΔE of relaxed $2p$ orbital energies compared to the atomic value are shown in Figure 9. We see here that ΔE decreases when T_e rises for each density considered, meaning that $2p$ orbital gets closer to the nucleus. This can be understood by the reduction of the electronic screening which leads to a more attractive electron-ion potential.

In these conditions, the highest shift of the $2p$ orbital is -2.3 eV for a temperature of 3 eV. This is almost the same value as the DOS shift illustrated on Figure 7, and this holds for all the temperatures shown here. This is why we do not observe a visible shift on the XANES spectra presented before in the Figures 3 and 4.

Regarding the density effect, $2p$ orbital energy also decreases when the density is lowered. Both the DOS (shown in Figure 6) and the $2p$ orbital move and almost in the same proportion (the maximum difference is 0.2 eV between the DOS and the $2p$ shifts at $\rho = 6$ g/cm^3), which results in an unchanged position of the XANES spectra.

IV. EXTRACTING T_e FROM X-RAY ABSORPTION SPECTRA

In warm dense Be [14] and Al [15], previous studies have demonstrated that the temperature induced K edge broadening could be fitted with a Fermi-Dirac distribution function to retrieve the value of the electronic temperature T_e. This methodology applies for relatively flat energy profile of the electron DOS. It cannot be used for copper whose DOS is dominated by the strongly localized $3d$-band.

We have evidenced that both density and temperature have influence on the electronic occupations dictated by $f(\epsilon, \mu(T_e))$. At the end, the variations in $\mu(T_e)$ and the resulting changes in $f(\epsilon, \mu(T_e))$ always lead to the depopulation of electrons of the $3d$-band, giving a pre–edge structure in the XANES spectra. The same phenomenon is observed for all the calculations we have performed, *i.e.* both (T_e,T_i)temperatures up to 3 eV, and densities ranging from solid density ρ_0 to densities as low as $\rho =$ 6 g/cm^3. The question is then can we use this pre–edge to deduce the value of the electronic temperature?

For this purpose, we consider the value of the spectral integral of the pre–edge. This integral is proportional to the number of unoccupied electronic states in the DOS. Figure 3 shows through the hatched area the energy region considered for such pre–edge integration (from 922.5 eV to 932.5 eV). The choice for integration region is arbitrary. The value of the integral of the cold spectrum in this spectral region is subtracted to the integral in each case. The integral is not equal to zero in the cold case even if no electron is thermally excited because of the spectral linewidth and the experimental broadening of the absorption edge. Spectral resolution and natural linewidth could modify the height this is why we choose to use the integral instead. Note that we compute the evolution of the pre-edge area refered to cold case. This, also, removed potential experimental resolution and natural linewidth effect assuming that there are the same for the different conditions explored here. Looking at the comparison between experimental and theoretical spectra for cold and hot conditions presented in figure 4.b in our previous paper [13], one can see that the agreement is really good for both temperatures showing that these approximations seem reasonable.

Using our *ab initio* XANES calculations performed for several temperatures at thermal equilibrium $T_e = T_i$, out-of-equilibrium $T_e \neq T_i$ and for three different copper densities, we have computed the value of the pre–edge integral for each spectrum and so for each electronic temperature T_e. The results are presented in the Figure 10. Below $T_e = 0.2$ eV, the pre–edge is too weak to be quantified and its evolution is not monotonous.Above 0.2 eV, the evolution of the pre–edge integral with T_e is monotonous. More remarkable, it does not depend significantly on the equilibrium versus non equilibrium condition, and depends little on the density. The amplitude of the pre-edge changes but not the area of the pre-edge.

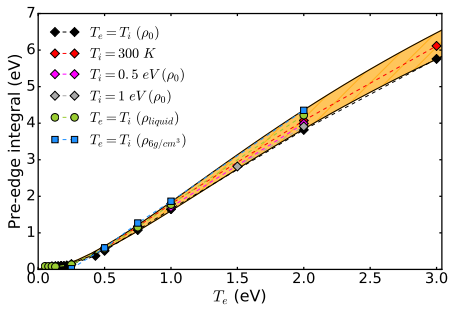


FIG. 10. (color online). Evolution of the pre–edge integral as a function of the electronic temperature T_e for all the simulated conditions.

At the end, the difference in the integral value reaches $\sim$ 15 % at 6 g/cm^3 compared to 8.9 g/cm^3.

Above $T_e = 0.2$ eV, as the evolution of the pre–edge integral is monotonous, it is possible to establish an unambiguous relationship between T_e and the pre–edge integral. This relationship has been recently used to measure the electron temperature dynamics of laser heated copper with a picosecond time resolution [13]. To be able to recover directly electronic temperature from experimental spectra, the requirement is to use for the integration exactly the same region as was chosen for theoretical spectra.

V. CONCLUSION

In summary, we calculated X-ray absorption spectra near $L_{2,3}$ edges of warm dense copper based on first principle electronic structure calculations and molecular dynamics simulations. By introducing a variable width to model the linewidth, we obtain a good description of the experimental XANES spectrum and its modulations at room temperature.

We explain the modifications induced by both electron and ion temperatures and density on XANES spectra at the microscopic level. The shape is modified in two ways. First, as copper is a noble metal with almost filled $3d$ states at ambient conditions, they do not appear on XANES spectrum near L edge at ambient condition. But, when the temperature of the electrons T_e increases, the $3d$ states are partially depopulated, leading to a pre–edge on the absorption spectrum and a reduction of the absorption behind the edge. The amplitude and shape of the pre–edge is directly linked to the modification of $3d$ electronic population. Second, the modulations above the edge disappear when the temperature increases as solid copper turns to a liquid state. This opens a promising perspective to the experimental study of phase transition dynamics in non-equilibrium warm dense transition metals. This observation would require further investigation. In the range of investigation (temperature up to 3 eV and density as low as 6 g/cm^3), we do not observe any energy shift of the XANES spectra, as the $2p$ core level shift is balanced by the DOS one.

The spectral integral of the pre–edge can be used to deduce the electronic temperature T_e for a wide range of temperatures and densities. This leads to a useful tool to associate an electronic temperature T_e to experimental XANES spectra. This tool can be used for any measurement of XANES spectra for femtosecond laser heated copper without the need of additional calculations keeping in mind that the same integral region has to be chosen to analyze the experimental spectra. The same considerations can be applied regarding the d-band of the other noble metals (Ag and Au). It could be possible to extract the electronic temperature in a similar way for other transition metals with localized d states.

We believe that for any material, there should be a direct connection between the electronic temperature and the shape on the XANES spectra. Then, there is always a way to directly *read* the temperature on XANES spectra. The signature will depends on the DOS. As soon as there is no localized states near the Fermi level, the temperature could be extracted directly by fitting a Fermi-Dirac function to the edge. If there is localized states near the Fermi level as for the transitions metals, the temperature will appear as a pre–edge or a shoulder. For all cases, one need first dedicated simulations to quantify the change induced by temperature.

ACKNOWLEDGMENTS

The authors are extremely grateful to M. Torrent for his precious help for the implementation in the ABINIT code.

[1] F. Dorchies and V. Recoules, Physics Reports **657**, 1 (2016).
[2] V. Recoules and S. Mazevet, Phys. Rev. B **80**, 064110 (2009).
[3] B. Cho, K. Engelhorn, A. Correa, T. Ogitsu, C. Weber, H. Lee, J. Feng, P. Ni, Y. Ping, A. Nelson, D. Prendergast, R. Lee, R. Falcone, and P. Heimann, Physical Review Letters **106**, 167601 (2011).
[4] P. Leguay, A. Lévy, B. Chimier, F. Deneuville, D. Descamps, C. Fourment, C. Goyon, S. Hulin, S. Petit, O. Peyrusse, J. Santos, P. Combis, B. Holst, V. Recoules, P. Renaudin, L. Videau, and F. Dorchies, Physical Review Letters **111**, 245004 (2013).
[5] F. Dorchies, V. Recoules, J. Bouchet, C. Fourment, P. Leguay, B. Cho, K. Engelhorn, M. Nakatsutsumi, C. Ozkan, T. Tschentscher, M. Harmand, S. Toleikis,

M. Störmer, E. Galtier, H. Lee, B. Nagler, P. Heimann, and J. Gaudin, Physical Review B **92**, 144201 (2015).
[6] A. Mancic, A. Lévy, M. Harmand, M. Nakatsutsumi, P. Antici, P. Audebert, P. Combis, S. Fourmaux, S. Mazevet, O. Peyrusse, V. Recoules, P. Renaudin, J. Robiche, F. Dorchies, and J. Fuchs, Physical Review Letters **104**, 035002 (2010).
[7] F. Dorchies, A. Lévy, C. Goyon, P. Combis, D. Descamps, C. Fourment, M. Harmand, S. Hulin, P. Leguay, S. Petit, O. Peyrusse, and J. Santos, Physical Review Letters **107**, 245006 (2011).
[8] A. Benuzzi-Mounaix, F. Dorchies, V. Recoules, F. Festa, O. Peyrusse, A. Lévy, A. Ravasio, T. Hall, M. Koenig, N. Amadou, E. Brambrink, and S. Mazevet, Physical Review Letters **107**, 165006 (2011).
[9] A. Lévy, F. Dorchies, A. Benuzzi-Mounaix, A. Ravasio, F. Festa, V. Recoules, O. Peyrusse, N. Amadou, E. Brambrink, T. Hall, M. Koenig, and S. Mazevet, Physical Review Letters **108**, 055002 (2012).
[10] C. Marini, F. Occelli, O. Mathon, R. Torchio, V. Recoules, S. Pascarelli, and P. Loubeyre, Journal of Applied Physics **115**, 093513 (2014).
[11] M. Harmand, A. Ravasio, S. Mazevet, J. Bouchet, A. Denoeud, F. Dorchies, Y. Feng, C. Fourment, J. G. E. Galtier, F. Guyot, R. Kodama, M. Koenig, H. Lee, K. Miyanishi, G. Morard, R. Musella, B. Nagler, M. Nakatsutsumi, N. Ozaki, V. Recoules, S. Toleikis, T. Vinci, U. Zastrau, D. Zhu, and A. Benuzzi-Mounaix, Physical Review B **92**, 024108 (2015).
[12] B. Cho, T. Ogitsu, K. Engelhorn, A. Correa, Y. Ping, J. W. Lee, L. J. Bae, D. Prendergast, , R. Falcone, and P. Heimann, Sci. Rep. **6**, 18843 (2015).
[13] N. Jourdain, L. Lecherbourg, V. Recoules, P. Renaudin, and F. Dorchies, Phys. Rev. B **97**, 075148 (2018).
[14] W. Schwanda and K. Eidmann, Phys. Rev. Lett. **69**, 3507 (1992).
[15] F. Dorchies, F. Festa, V. Recoules, O. Peyrusse, A. Benuzzi-Mounaix, E. Brambrink, A. Levy, A. Ravasio, M. Koenig, T. Hall, and S. Mazevet, Physical Review B **92**, 085117 (2015).
[16] The Abinit code is a common project of the Université Catholique de Louvain, Corning Incorporated, Commissariat à l'Energie Atomique, Université de Liège, Mitsubishi Chemical Corp. and other contributions, "http://www.abinit.org,".
[17] X. Gonze, B. Amadon, P. Anglade, J. Beuken, F. Bottin, P. Boulanger, F. Bruneval, D. Caliste, R. Caracas, M. Côté, T. Deutsch, L. Genovese, P. Ghosez, M. Giantomassi, S. Goedecker, D. Hamann, P. Hermet, F. Jollet, G. Jomard, S. Leroux, M. Mancini, S. Mazevet, M. Oliveira, G. Onida, Y. Pouillon, T. Rangela, G. Rignanese, D. Sangalli, R. Shaltaf, M. Torrent, M. Verstraete, G. Zerah, and J. Zwanziger, Computer Physics Communications **180**, 2582 (2009).
[18] F. Bottin, S. Leroux, A. Knyazev, and G. Zerah, Computational Materials Science **42**, 329 (2008).
[19] J. P. Perdew and Y. Wang, Phys. Rev. B **45**, 13244 (1992).
[20] A. Dewaele, M. Torrent, P. Loubeyre, and M. Mezouar, Phys. Rev. B **78**, 104102 (2008).
[21] M. Taillefumier, D. Cabaret, A. Flank, and F. Mauri, Physical Review B **66**, 195107 (2002).
[22] O. Bunau and M. Calandra, Physical Review B **87**, 205105 (2001).
[23] N. Holzwarth, A. Tackett, and G. Matthews, Computer Physics Communications **135**, 329 (2001).
[24] V. Mauchamp, M. Jaouen, and P. Schattschneider, Physical Review B **79**, 235106 (2009).
[25] M. O. Krausse and J. H. Oliver, J. Chem. Ref. Data **8**, 329 (1979).
[26] T. Miyamoto, H. Niinmi, Y. Kitajima, and K. Asakura, Coordination Chemistry Review **272-278**, 44 (2014).
[27] B. Holst, V. Recoules, S. Mazevet, M. Torrent, A. Ng, Z. Chen, S. E. Kirkwood, V. Sametoglu, M. Reid, and Y. Y. Tsui, Phys. Rev. B **90**, 035121 (2014).
[28] E. Bevillon, J. Colombier, V. Recoules, and R. Stoian, Physical Review B **89**, 115117 (2014).